

DETECTING AND CORRECTING ADVERSARIAL IMAGES USING IMAGE PROCESSING OPERATIONS AND CONVOLUTIONAL NEURAL NETWORKS

Huy H. Nguyen^{*}, Minoru Kuribayashi[§], Junichi Yamagishi^{*†#}, and Isao Echizen^{*†‡}

^{*}The Graduate University for Advanced Studies, SOKENDAI, Kanagawa, Japan

[§]Graduate School of Natural Science and Technology, Okayama University, Okayama, Japan

[†]National Institute of Informatics, Tokyo, Japan; [‡]The University of Tokyo, Tokyo, Japan

[#]The University of Edinburgh, Edinburgh, UK

Email: {nhhuy, jyamagis, iechizen}@nii.ac.jp; kminoru@okayama-u.ac.jp

ABSTRACT

Deep neural networks (DNNs) have achieved excellent performance on several tasks and have been widely applied in both academia and industry. However, DNNs are vulnerable to adversarial machine learning attacks, in which noise is added to the input to change the network output. We have devised two methods for detecting adversarial images; one based on statistical image processing and one based on convolutional neural network in which the final softmax layer is removed during training. In addition to detection, the image-processing-based method can be used to reduce adversarial noise in images and thereby restore the image labels, which is crucial to restoring the normal functionalities of DNN-based systems. Testing using an adversarial machine learning database we created for generating several types of attack using images from the ImageNet Large Scale Visual Recognition Challenge database demonstrated the efficiency of our proposed methods for both detection and correction even when training was done from scratch on a small database.

Index Terms— adversarial machine learning, detecting adversarial image, correcting adversarial image, convolutional neural network

1. INTRODUCTION

Although adversarial machine learning is not a new issue in the machine learning community, as it was first discussed in 2004 [1], it has recently become a major concern due to the advances made in deep learning that have made deep neural networks (DNNs) vulnerable to adversarial attacks [2]. Besides traditional logical attacks, in which adversarial noise is added to image or audio files, attackers can now create physical adversarial examples [3, 4, 5, 6]. When autonomous systems have become mainstream in both the research community and industry, physical adversarial attacks may threaten their safety and reliability. Besides white-box attacks, in which attackers have full knowledge of the inner configuration of the target models, attackers will also be able to perform black-box attacks, which are more likely since attackers need only acquire only the models' outputs [7].

Several countermeasures have been proposed for detecting adversarial examples such as statistical testing [8], directly detecting pixels in input images [9], detecting using features from intermediate layers of the targeted DNN [10], and applying statistical analysis to the outputs of the intermediate layers [11]. Xu et al. used feature squeezing to reduce the search space available to an adversary which was useful for detection [12]. Besides detection, there have

been several attempts to harness the DNN models in training by using distillation [13], obfuscating gradients [14], or applying the reverse cross-entropy loss function [15]. Several adversarial databases have been independently created for use in evaluating the proposed methods, but detailed guidelines for creating them have not been reported. Although the robustness of adversarial noise has been discussed [3, 12], a method for correcting adversarial images has not been reported.

In this paper, **first**, we present the procedure we used for creating an adversarial database using images from the ImageNet Large Scale Visual Recognition Challenge (ILSVRC) 2012 validation set [16]. We used the FoolBox library [17] to create adversarial images for two types of attack: targeted attacks, which force the outputs to become target labels, and non-targeted attacks, which force the top-5 outputs to not include certain labels [7] (discussed in section 2). **Second**, we discuss the measured effects of some image processing operations on both normal and adversarial images given the hypothesis that adversarial noise is reduced, resulting in the classification labels of the adversarial images being changed while the normal images almost remain unaffected. This measurement was motivated by the work of Kurakin et al. [3] and Xu et al. [12]. We also discuss the use of these operations to detect adversarial images on the basis of statistics and to correct their labels as classified by the targeted object recognition DNNs (discussed in section 3). **Third**, we present a training strategy for use with a convolutional neural network (CNN) based method for detecting adversarial images by omitting the final softmax layer [18], which increases detection accuracy (discussed in section 4).

2. CREATING ADVERSARIAL DATABASE

2.1. Overview

We used images from the ILSVRC 2012 validation set [16] (which has labeled ground truths) to generate the adversarial images used in our experiments. For the object recognition CNNs, we used pre-trained VGG-16 and -19 networks (as proposed by the Visual Geometry Group) [19] and pre-trained ResNet-18 and -50 networks (as proposed by Microsoft Research) [20], implemented using the PyTorch framework [21]. We used the Pillow library¹ for image processing and the FoolBox library (version 1.8.0) [17] for adversarial image generation. Twelve commonly used methods (Table 1) were used to perform targeted and non-targeted adversarial attacks.

¹<https://pillow.readthedocs.io/en/stable>

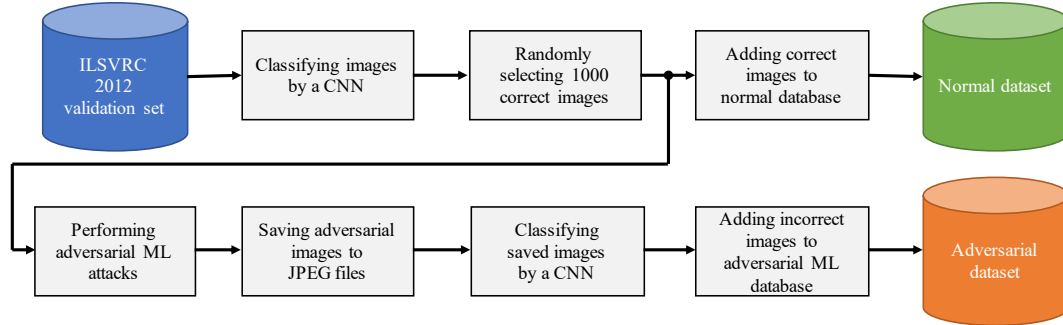


Fig. 1. Overview of data generation procedure using a CNN. The same procedure was used with VGG-16, VGG-19, ResNet-18, and ResNet-50 networks in order to create a complete normal dataset (for normal images) and an adversarial dataset (for adversarial images).

An overview of the procedure we used is shown in Fig. 1. We used each CNN to classify 5 million images from the ILSVRC 2012 validation set. We then randomly selected 1000 images per CNN that were correctly classified (the ground-truth labels were among the predicted top-5 results). Only 1000 image per CNN were selected due to the time required to create adversarial images from them. The selected images were added to the normal dataset. We then performed the 12 adversarial attacks listed in Table 1 on the selected images and selected misclassified ones (those for which the predicted top-5 results did not contain the previously predicted labels). The Pillow library was used to save them as JPEG files with a quality factor of 100 to ensure that the attack was close to a real-world scenario since adversarial noise can be lost when saving adversarial images to a file. We then loaded the saved images and used the same CNN to classify them again to ensure that they were still misclassified. The misclassified adversarial images were then added to the adversarial dataset. This procedure was also used with VGG-16, VGG-19, ResNet-18, and ResNet-50 networks.

2.2. Creating Adversarial Images and Database

For targeted attacks, we used the limited-memory Broyden-Fletcher-Goldfarb-Shanno (L-BFGS) method proposed by Szegedy et al. [2], the basic iterative method (BIM), which uses L-infinity, the projected gradient descent (PGD) method described by Kurakin et al. [3], and the L1- and L2- versions of BIM (L1-iter and L2-iter) implemented in FoolBox [17]. Since the ILSVRC 2012 validation set has 1000 labels, the target label index for each adversarial image was its 100-step-right-shifted top-1 predicted label index (calculated using the target CNN). Modular operation was used to ensure the shifted label index was in the range $[0, 1000)$. The attack criteria for the target class probability was 99%.

For non-targeted attacks, we used the basic gradient attack method implemented in FoolBox [17], the fast gradient signed method (FGSM) proposed by Goodfellow et al. [22], the Deep Fool method proposed by Moosavi-Dezfooli et al. [23], the Newton method proposed by Jang et al. [24], the ADef method proposed by Alaifari et al. [25], the Saliency Map method proposed by Papernot et al. [26], and the attack method proposed by Carlini and Wagner [27]. Since these methods are non-targeted attacks, the attack criterion was to change the predicted top-5 labels so that they were different from the original predicted top-1 labels.

As shown by the results in Table 1, the VGG networks were generally more vulnerable to targeted attacks than the ResNet networks, resulting in a larger numbers of misclassified images. The modified

Table 1. Number of successful adversarial images created using FoolBox library [17] on VGG-16, VGG-19, ResNet-18, and ResNet-50 networks.

Method	VGG-16	VGG-19	ResNet-18	ResNet-50
Targeted attacks:				
L-BFGS [2]	618	623	348	229
BIM [3]	693	711	531	431
PGD [3]	651	678	484	348
L1-iter [17]	661	591	680	513
L2-iter [17]	820	746	722	583
Non-targeted attacks:				
Gradient [17]	654	548	590	517
FGSM [22]	509	450	451	379
Deep Fool [23]	707	671	658	604
Newton [24]	571	505	558	425
ADef [25]	1	4	1	1
Saliency Map [26]	102	86	114	71
Carlini-Wagner [27]	427	361	401	299

BIM attack using the L2 distance (L2-iter) was the most effective attack overall. The non-targeted attacks were more difficult to carry out since they needed to change the top-5 labels so that they did not include the current top-1 labels. Among them, Deep Fool was the most successful while the ADef attack was the least successful overall, producing only one or four adversarial images for each network. The Saliency Map attack also had limited success, with around 100 adversarial images for each network.

Table 2. Details of normal and adversarial image datasets, which were divided into training, development, and evaluation sets.

Dataset	Normal	Adversarial	Total	Ratio
Train	2,800	16,110	18,910	1:5.75
Dev	600	3,092	3,692	1:5.15
Eval	600	3,124	3,724	1:5.21

We mixed together the 1000 normal images from each classifier and the created adversarial images and divided them into training (train), development (dev), and evaluation (eval) sets at an approximate ratio of 7.0:1.5:1.5, as detailed in Table 2. The train set was used for training, the dev set was used to select the model, and the eval set was used to test the classifiers. We ensured that the normal images and their adversarial versions in the three sets did not overlap so that the classifier would not remember the training images. We did not focus on detecting adversarial images created by unseen adversarial attacks, so the images from each attack had equal prob-

abilities of appearing in the three sets. The number of adversarial images was more than five times that of normal images.

3. EFFECTS OF IMAGE PROCESSING OPERATIONS ON NORMAL AND ADVERSARIAL IMAGES AND THEIR APPLICATIONS

In section 3.1, we describe the effects of applying four image processing operations to images (normal and adversarial) on the top-5 classification results for VGG-16, VGG-19, ResNet-18, and ResNet-50 networks. Differences in behavior between normal and adversarial images were identified, and these differences could be useful for detecting (section 3.2) and correcting adversarial images (section 3.3).

3.1. Effects of Image Processing Operations on Normal and Adversarial Images

We extended the ideas of Kurakin et al. [3] and Xu et al. [12] by measuring the change in the top-5 labels after applying four image processing operations with various parameters (listed below) to normal and adversarial images.

- JPEG compression with quality $\in \{100, 95, 90, 85, 80, 75, 70, 65, 60, 55, 50, 45, 40, 35, 30, 25\}$.
- Gaussian blur with kernel size $\in \{2, 3, 4, 5\}$.
- Clockwise image rotation with angle $\in \{1^\circ, 2^\circ, 3^\circ, 4^\circ, 5^\circ, 6^\circ, 7^\circ, 8^\circ\}$ and without reversing back.
- Image scaling with scale $\in \{0.75, 0.8, 0.85, 0.9, 0.95, 1.05, 1.1, 1.15, 1.2, 1.25\}$ and without reversing back.

The image operations were done using Pillow version 6.1.0. Some of the results for ResNet-18 are shown in Table 3. Similar behaviors were also observed for VGG-16, VGG-19, and ResNet-50. The JPEG compression with quality 100 changed the top-5 labels for both the normal and adversarial images, however its effect on adversarial images was clearer. Reducing image quality by increasing the compression ratio greatly reduced the number of misclassified adversarial images and slightly increased that of misclassified normal images. A large increase in the compression ratio increased the misclassification rate for normal images. The results for scaling, Gaussian blur, and rotation were similar to those for compression. One result in particular should be noted: the number of misclassified normal images after applying 3×3 Gaussian blur kernel was higher than after applying the other operations, which is not good for our purposes.

3.2. Detecting Adversarial Images using Statistical Features

As mentioned above, the differences in behavior between normal and adversarial images for the top-5 labels when the four image processing operations are applied may be useful for detecting adversarial images. We thus propose using two features for detecting adversarial images: a counting feature and a differences feature. First, we define three variables.

- $L = (a, b, c, d, e)$: top-5 label for image I (normal or adversarial) predicted using a CNN before applying image processing operation i (e.g., JPEG compression with a quality of 80 or 5° clockwise rotation).
- $L_i = (a_i, b_i, c_i, d_i, e_i)$: top-5 label for an image after applying image processing operation i .
- n : total number of image processing operations (38 in our experiments).

3.2.1. Counting feature

Let us call $C(a)$ the number of occurrences of label $a \in L = (a, b, c, d, e)$ at the first position in an ordered top-5 label set $\{L_i | i = 1..n\}$ and $\mathbb{1}(\cdot)$ the counting function. $C(a)$ is defined as

$$C(a) = \sum_{i=1}^n \mathbb{1}(a_i = a). \quad (1)$$

The same equation is used for b, c, d , and e at the second, third, fourth, and fifth positions, respectively. Therefore, the features of each image are $\{C(a), C(b), C(c), C(d), C(e)\}$.

3.2.2. Differences feature

Let us call $\Delta(a, a_i)$ the binary differential function used to measure the difference between two labels, a and a_i :

$$\Delta(a, a_i) = \begin{cases} 1, & \text{if } a_i \neq a \\ 0, & \text{if } a_i = a. \end{cases} \quad (2)$$

The differences feature derived from input image I can be expressed as the set

$$\{(\Delta(a, a_i), \Delta(b, b_i), \Delta(c, c_i), \Delta(d, d_i), \Delta(e, e_i)) | i = 1..n\}.$$

3.2.3. Detecting adversarial images using image-processing-based features

Using the two features introduced above, we evaluated the performance of detectors using one of the four classifiers: the C-support vector classification (SVC) version of the support vector machine (SVM) classifier [28], the random forest classifier [29] with 100 estimators and a maximum depth of 2, the linear discriminant analysis (LDA) classifier [30], and the multiple layer perception (MLP) classifier [31]. All of them were implemented in the scikit-learn library version 0.21.3².

As shown in Table 4, the differences feature produced slightly higher accuracies than the counting feature (which was smaller than the differences feature). Among the individual image processing operations, the scaling one achieved the highest accuracy for all detectors. Also as shown in the table, the combination of JPEG compression and scaling and the combination of all operations resulted in higher accuracy than using any of them separately. However, these combinations also increased the feature size and more classification operations were required of the CNNs (VGG-Nets or ResNets) to produce those features. For the counting feature, using the MLP-based detector on the features from JPEG compression and the scaling operation resulted in the highest accuracy (93.56%) while for the differences feature, using the SVM-based detector on all features from all image processing operations resulted in the highest accuracy (94.20%).

3.3. Correcting Adversarial Images

Given that the image processing operations substantially reduced the number of misclassified adversarial images, they could also be useful in restoring the original labels of the images in addition to classifying them. Those operations helped mitigate the adversarial noise while only slightly affecting the normal images. Since there are several kinds of adversarial attacks, we focused on correcting noise-based

²<https://scikit-learn.org/stable>

Table 3. Number of top-5 misclassified images for ResNet-18 network from both normal and adversarial datasets before and after applying image processing operations.

Attack	Original	JPEG Compression					Scaling						Gaussian	Rotation	
		100	80	60	40	20	0.75	0.85	0.95	1.05	1.15	1.25	3×3	2°	5°
Normal images	0	6	29	50	59	108	93	44	34	26	52	35	329	54	75
Targeted attack:															
L-BFGS [2]	348	341	41	50	58	67	88	58	44	59	68	42	63	61	92
BIM [3]	531	529	52	54	69	88	103	66	55	65	84	47	87	72	101
PGD [3]	484	479	45	50	61	82	102	60	53	61	77	42	77	65	95
L1-iter [17]	680	676	60	62	61	81	100	71	65	80	92	60	93	91	115
L2-iter [17]	722	720	66	59	72	88	107	72	69	88	99	60	100	99	123
Non-targeted attack:															
Gradient [17]	590	584	107	76	66	95	93	70	75	115	122	86	108	105	155
FGSM [22]	451	449	109	87	76	101	99	67	79	125	124	93	95	110	158
Deep Fool [23]	658	645	83	55	51	72	60	51	59	74	72	46	59	80	50
Newton [24]	558	552	118	61	60	74	62	61	64	90	82	48	82	105	68
ADef [25]	1	1	1	1	1	0	0	0	0	0	0	0	0	0	0
Saliency Map [26]	114	109	42	41	40	54	59	40	28	36	38	27	33	43	44
Carlini-Wagner [27]	401	391	59	50	48	75	68	43	42	59	59	45	38	67	49

Table 4. Accuracy (in %) of each classifier using counting feature (count) and difference feature (diff.) on eval set.

Classifier	JPEG		Scaling		Gaussian Blur		Rotation		JPEG + Scaling		All	
	Count	Diff.	Count	Diff.	Count	Diff.	Count	Diff.	Count	Diff.	Count	Diff.
SVM (SVC) [28]	90.98	91.92	92.56	92.32	87.35	87.35	89.90	89.39	92.86	94.04	93.39	94.20
Random forest [29]	90.57	89.82	91.08	91.27	86.87	86.04	88.24	88.59	92.16	91.94	92.35	92.35
LDA [30]	89.98	90.36	91.97	91.62	85.77	87.35	89.15	89.29	92.86	92.67	92.21	92.86
MLP [31]	91.25	90.41	92.32	92.35	86.95	87.38	89.66	89.02	93.56	92.19	93.37	92.29

adversarial images. The correction task is usually performed after adversarial image detection. In this section, we introduce our proposed correction method and the experiment results.

3.3.1. Proposed correction method

Let us call $\mathbf{S} = \{L_i | i = 1..n\}$ the set of top-5 labels acquired by applying n image processing operations to image I . We calculated the frequencies of every label in \mathbf{S} and identified the five labels with the highest frequencies. These labels were the corrected top-5 ones.

3.3.2. Evaluation

Since there were false positive inputs, i.e., normal images misclassified as adversarial images, we tested our correction method on both normal and adversarial images. We used our entire database for testing. For the image processing operations, we used JPEG compression, scaling, and their combination. As shown in Table 5, JPEG compression had better performance than scaling operation for the adversarial images, and their combination produced the best performance. Only 1.88% of the normal images was misclassified after “correction” while 89.91% of the adversarial images were corrected. If we performed this correction after detection of adversarial images, 98.12% of the false positive inputs (normal images misclassified as adversarial ones) would also be corrected.

4. DETECTING ADVERSARIAL IMAGES USING CONVOLUTIONAL NETWORKS

In addition to using handcrafted features like those used in our proposed detection method (section 3.2) to detect adversarial images, CNNs are widely used [7]. Since they are hard to train on small

Table 5. Percentage of corrected top-5 classifications after applying proposed correction method to both normal and adversarial images.

Operation(s)	Normal Images	Adversarial Images
JPEG compression	96.30	88.63
Scaling	97.82	85.69
Both	98.12	89.91

databases, fine-tuning pre-trained networks from a different task (usually object recognition) is a better choice. The results shown in Table 6 show that the performances of such networks were approximately the same as those of our proposed image-processing-based method while revealing their potential vulnerability to a second-level adversarial attack (an adversarial attack targeting adversarial image detectors). To make CNN-based adversarial detectors a better choice with higher performance, we devised a training strategy that makes the training process easier and that results in higher accuracies. The strategy is simple: omit the final softmax layer [18] during training. We still used it during evaluation (test mode) to convert the output into a probability.

Let us call y the ground-truth label (1 for adversarial images and 0 for normal images) and \hat{y}_{adv} and \hat{y}_{norm} the logits representing adversarial images and normal images, respectively, which were calculated by a detector. These logits were not limited to the range $[0, 1]$. For normal training, the softmax layer is used to convert these logits into probabilities before feeding them into a cross-entropy loss. In our case, we tried to minimize the loss in equation 3. Since there was no constraint on the range of logit values, the optimizer encouraged the network to produce logits with greater separation between the adversarial and normal images.

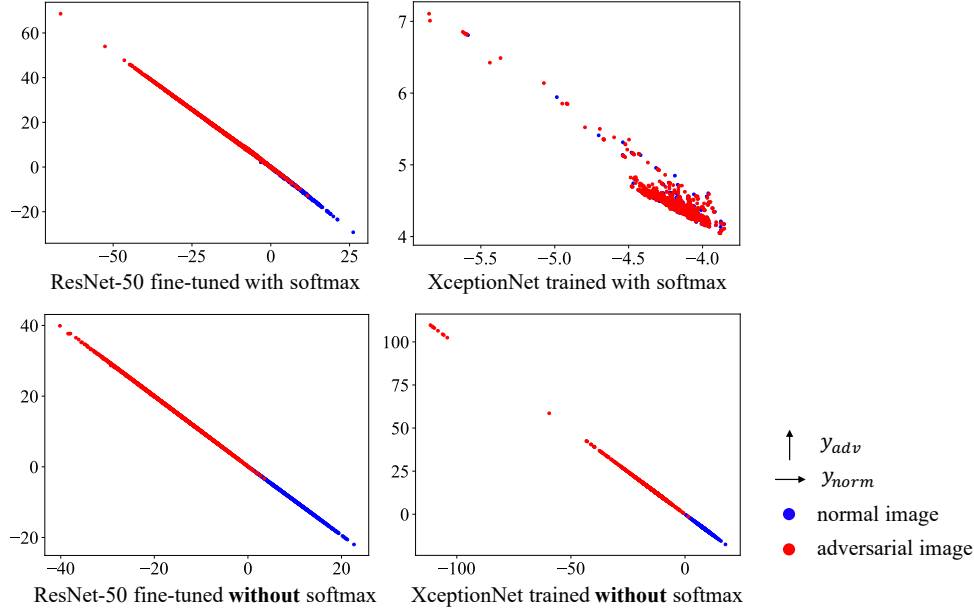


Fig. 2. Visualization of logits of ResNet-50 and XceptionNet on the test set of adversarial image database. ResNet-50 was fine-tuned while XceptionNet was trained from scratch with and without final softmax layer. Red dots indicate adversarial input images while blue dots indicate normal input images.

$$\mathcal{L} = -y \log(\hat{y}_{adv}) - (1 - y) \log(\hat{y}_{norm}) \quad (3)$$

We used two commonly used CNN architectures for evaluation: ResNet-50 [20] and XceptionNet [32]. We tried both fine-tuning the ILSVRC pre-trained versions and training them from scratch. We used a learning rate of $5e^{-4}$ for all cases except fine-tuning the two networks with the final softmax layer, in which case we used a lower rate ($5e^{-5}$) to make these networks converge. The results are shown in Table 6. With the final softmax layer, training both networks from scratch was difficult, and the results were poor with high equal error rates (EERs). Without the final softmax layer, we achieved the highest accuracies when fine-tuning both networks and even when training the XceptionNet from scratch, which had the best performance among all detectors. The superior result from XceptionNet reveals a big advantage of our proposed method: a pre-trained model is not needed even with a small adversarial image database.

The visualizations of the logits of ResNet-50 and XceptionNet on the test set of our adversarial image database in Fig 2 confirm our hypothesis. With ResNet-50 and fine-tuning, training without the final softmax layer reduced the overlap between classes. For XceptionNet, training from scratch with the final softmax layer did not result in convergence since there was no separation between classes, leading to an EER of nearly 50%. Without the final softmax layer, there was strong separation between adversarial and normal images with the origin (0, 0) on the boundary.

5. SUMMARY AND FUTURE WORK

Both a statistical-based detector using image processing operations and a CNN-based detector demonstrated the ability to detect adversarial images with high accuracy. When the final softmax layer was omitted during training, CNN-based detectors had the best performance even when training on a small database. Our proposed image-

Table 6. Accuracy and EER (in %) of each detector on eval set. The first two detectors were the best ones based on the results presented in the previous section. The next four were baselines, and the last four are our proposed methods, which do not use the final softmax layer in training.

Detector	Accuracy	EER
MLP - counting feature	93.56	10.50
SVM - differences feature	94.20	9.67
ResNet-50 (training)	83.89	48.00
ResNet-50 (fine-tuning)	93.29	9.00
XceptionNet (training)	83.89	49.33
XceptionNet (fine-tuning)	92.59	15.23
ResNet-50 (training - no softmax)	83.89	49.09
ResNet-50 (fine-tuning - no softmax)	99.49	0.66
XceptionNet (training - no softmax)	99.95	0.15
XceptionNet (fine-tuning - no softmax)	99.60	0.49

processing-based method for restoring the original labels of adversarial images can be used together with the proposed detectors to improve the performance of DNNs under adversarial attack. Future work will address more adversarial attacks on larger and more diverse databases along with reducing the number of image processing operations in order to reduce computational expense.

Acknowledgements

This research was supported by JSPS KAKENHI Grants JP16H06302, JP17H04687, JP18H04120, JP18H04112, JP18KT0051, JP19K22846, and by JST CREST Grant JP-MJCR18A6, Japan.

References

- [1] Nilesh Dalvi, Pedro Domingos, Sumit Sanghai, Deepak Verma, et al., “Adversarial classification,” in *PSIGKDD*. ACM, 2004, pp. 99–108.
- [2] Christian Szegedy, Wojciech Zaremba, Ilya Sutskever, Joan Bruna, Dumitru Erhan, Ian Goodfellow, and Rob Fergus, “Intriguing properties of neural networks,” *arXiv preprint arXiv:1312.6199*, 2013.
- [3] Alexey Kurakin, Ian Goodfellow, and Samy Bengio, “Adversarial examples in the physical world,” in *ILCR-W*, 2017.
- [4] Kevin Eykholt, Ivan Evtimov, Earlene Fernandes, Bo Li, Amir Rahmati, Florian Tramer, Atul Prakash, Tadayoshi Kohno, and Dawn Song, “Physical adversarial examples for object detectors,” in *WOOT*, 2018.
- [5] Adith Bloor, Xin He, Christopher Gill, Yevgeniy Vorobeychik, and Xuan Zhang, “Simple physical adversarial examples against end-to-end autonomous driving models,” *arXiv preprint arXiv:1903.05157*, 2019.
- [6] Lea Schönherr, Katharina Kohls, Steffen Zeiler, Thorsten Holz, and Dorothea Kolossa, “Adversarial attacks against automatic speech recognition systems via psychoacoustic hiding,” in *NDSS*, 2019.
- [7] Han Xu, Yao Ma, Haochen Liu, Debayan Deb, Hui Liu, Jiliang Tang, and Anil Jain, “Adversarial attacks and defenses in images, graphs and text: A review,” *arXiv preprint arXiv:1909.08072*, 2019.
- [8] Kathrin Grosse, Praveen Manoharan, Nicolas Papernot, Michael Backes, and Patrick McDaniel, “On the (statistical) detection of adversarial examples,” *arXiv preprint arXiv:1702.06280*, 2017.
- [9] Zhitao Gong, Wenlu Wang, and Wei-Shinn Ku, “Adversarial and clean data are not twins,” *arXiv preprint arXiv:1704.04960*, 2017.
- [10] Jan Hendrik Metzen, Tim Genewein, Volker Fischer, and Bastian Bischoff, “On detecting adversarial perturbations,” in *ICLR*, 2017.
- [11] Xin Li and Fuxin Li, “Adversarial examples detection in deep networks with convolutional filter statistics,” in *CVPR*, 2017, pp. 5764–5772.
- [12] Weilin Xu, David Evans, and Yanjun Qi, “Feature squeezing: Detecting adversarial examples in deep neural networks,” in *NDSS*, 2018.
- [13] Nicolas Papernot, Patrick McDaniel, Xi Wu, Somesh Jha, and Ananthram Swami, “Distillation as a defense to adversarial perturbations against deep neural networks,” in *SP*. IEEE, 2016, pp. 582–597.
- [14] Anish Athalye, Nicholas Carlini, and David Wagner, “Obfuscated gradients give a false sense of security: Circumventing defenses to adversarial examples,” in *ICLR*, 2018, pp. 274–283.
- [15] Tianyu Pang, Chao Du, Yinpeng Dong, and Jun Zhu, “Towards robust detection of adversarial examples,” in *NeurIPS*, 2018, pp. 4579–4589.
- [16] Olga Russakovsky, Jia Deng, Hao Su, Jonathan Krause, Sanjeev Satheesh, Sean Ma, Zhiheng Huang, Andrej Karpathy, Aditya Khosla, Michael Bernstein, Alexander C. Berg, and Li Fei-Fei, “ImageNet Large Scale Visual Recognition Challenge,” *IJCV*, vol. 115, no. 3, pp. 211–252, 2015.
- [17] Jonas Rauber, Wieland Brendel, and Matthias Bethge, “Foolbox: A python toolbox to benchmark the robustness of machine learning models,” *arXiv preprint arXiv:1707.04131*, 2017.
- [18] Ian Goodfellow, Yoshua Bengio, and Aaron Courville, *Deep Learning*, MIT Press, 2016, <http://www.deeplearningbook.org>.
- [19] Karen Simonyan and Andrew Zisserman, “Very deep convolutional networks for large-scale image recognition,” in *CLR*, 2015.
- [20] Kaiming He, Xiangyu Zhang, Shaoqing Ren, and Jian Sun, “Deep residual learning for image recognition,” in *CVPR*, 2016, pp. 770–778.
- [21] Adam Paszke, Sam Gross, Soumith Chintala, Gregory Chanan, Edward Yang, Zachary DeVito, Zeming Lin, Alban Desmaison, Luca Antiga, and Adam Lerer, “Automatic differentiation in pytorch,” in *NIPS-W*, 2017.
- [22] Ian J Goodfellow, Jonathon Shlens, and Christian Szegedy, “Explaining and harnessing adversarial examples,” *arXiv preprint arXiv:1412.6572*, 2014.
- [23] Seyed-Mohsen Moosavi-Dezfooli, Alhussein Fawzi, and Pascal Frossard, “Deepfool: a simple and accurate method to fool deep neural networks,” in *CVPR*, 2016, pp. 2574–2582.
- [24] Uyeong Jang, Xi Wu, and Somesh Jha, “Objective metrics and gradient descent algorithms for adversarial examples in machine learning,” in *ACSAC*. ACM, 2017, pp. 262–277.
- [25] Rima Alaifari, Giovanni S Alberti, and Tandri Gauksson, “ADef: an iterative algorithm to construct adversarial deformations,” in *ILCR*, 2019.
- [26] Nicolas Papernot, Patrick McDaniel, Somesh Jha, Matt Fredrikson, Z Berkay Celik, and Ananthram Swami, “The limitations of deep learning in adversarial settings,” in *EuroS&P*. IEEE, 2016, pp. 372–387.
- [27] Nicholas Carlini and David Wagner, “Towards evaluating the robustness of neural networks,” in *SP*. IEEE, 2017, pp. 39–57.
- [28] Corinna Cortes and Vladimir Vapnik, “Support-vector networks,” *Machine learning*, vol. 20, no. 3, pp. 273–297, 1995.
- [29] Tin Kam Ho, “Random decision forests,” in *ICDAR*. IEEE, 1995, vol. 1, pp. 278–282.
- [30] Richard O Duda, Peter E Hart, David G Stork, et al., *Pattern classification*, vol. 2, Wiley New York, 1973.
- [31] Dennis W Ruck, Steven K Rogers, Matthew Kabrisky, Mark E Oxley, and Bruce W Suter, “The multilayer perceptron as an approximation to a bayes optimal discriminant function,” *IEEE Transactions on Neural Networks*, vol. 1, no. 4, pp. 296–298, 1990.
- [32] François Chollet, “Xception: Deep learning with depthwise separable convolutions,” in *CVPR*, 2017, pp. 1251–1258.